Contiguous Binding of Decylsulfate on the Interface-Binding Surface of Pancreatic Phospholipase A_2

Shi Bai,[‡] Mahendra K. Jain,*[,‡] and Otto G. Berg[§]

Department of Chemistry and Biochemistry, University of Delaware, Newark, Delaware 19716, and Department of Molecular Evolution, Evolutionary Biology Center, Uppsala University, Uppsala, Sweden

Received October 29, 2007; Revised Manuscript Received January 16, 2008

ABSTRACT: Pig pancreatic IB phospholipase A_2 (PLA2) forms three distinguishable premicellar $E_i^\#$ ($i = 1$, 2, and 3) complexes at successively higher decylsulfate concentrations. The Hill coefficient for $E_1^\#$ is $n_1 = 1.6$, and n_2 and n_3 for $E_2^\#$ and $E_3^\#$ are about 8 each. Saturation-transfer difference nuclear magnetic resonance (NMR) and other complementary results with PLA2 show that decylsulfate molecules in $E_2^\#$ and $E_3^\#$ are contiguously and cooperatively clustered on the interface-binding surface or i-face that makes contact with the substrate interface. In these complexes, the saturation-transfer difference NMR signatures of ^1H in decylsulfate are different. The decylsulfate epitope for the successive $E_i^\#$ complexes increasingly resembles the micellar complex formed by the binding of PLA2 to preformed micelles. Contiguous cooperative amphiphile binding is predominantly driven by the hydrophobic effect with a modest electrostatic shielding of the sulfate head group in contact with PLA2. The formation of the complexes is also associated with structural change in the enzyme. Calcium affinity of $E_2^\#$ appears to be modestly lower than that of the free enzyme and $E_1^\#$. Binding of decylsulfate to the i-face does not require the catalytic calcium required for the substrate binding to the active site and for the chemical step. These results show that $E_i^\#$ complexes are useful to structurally characterize the cooperative sequential and contiguous binding of amphiphiles on the i-face. We suggest that the allosteric changes associated with the formation of discrete $E_i^\#$ complexes are surrogates for the catalytic and allosteric states of the interface activated PLA2.

The processive interfacial catalytic turnover rate by secreted pig pancreatic IB phospholipase A_2 (PLA2)[1] on bilayer and micelles of anionic phospholipid substrates is orders of magnitude larger than the rate with monodisperse (*1*) or aggregated (*2–6*) zwitterionic substrates. Analyses of the elementary events within the interfacial kinetic paradigm (*5, 6*) show that the preference of PLA2 for the anionic interface (*7–10*) has three contributions. First, the high-affinity binding of PLA2 along the i-face to the substrate interface increases the residence time of the interface-activated E* for the processive interfacial turnover (*4, 10*−*12*). Second, the substrate affinity for the active site of E* is 10−100-fold larger than that for the solution form, the E form, as the basis for K_s^* activation (*13, 14*). Third, the 15-fold k_{cat}^* activation by the anionic interface is attributed to the charge compensation of K53, K56, and K120 (*14–16*). Results with mutants of PLA2 (*7, 17*) and the kinetic effects of bile salts (*18*) suggest that the highly conserved hydrogen-bonding network (*19*) and the 57–71 loop participate in the allosteric coupling of the active-site events to the cooperative amphiphile binding along the i-face.

Atomic level characterization of the interface-activated form of PLA2 is challenging. A model for interactions of amphiphiles with the active site and i-face is pieced together from complementary results. The active-site and i-face (Figure 1) interactions of PLA2 occur over a relatively flat surface of 1600 Å^2 area that makes tight contact with about 30 phospholipid molecules on the anionic interface (*5, 7*−*9, 20*−*23*). The desolvated contact of the i-face with amphiphile head groups is stabilized by short-range specific interactions between polarizable ligands. The enthalpy contribution of such ligand-exchange reactions and the resulting hydrophobic effect would desolvate the contact surface without disrupting the bilayer organization (*7, 20, 24*).

Studies with premicellar $E_i^\#$ complexes of interfacial enzymes (*1, 5, 6, 14, 25*) provide additional insights into amphiphile interactions along the i-face and their coupling to active-site events (*19, 26–29*). The thermodynamic rationale for the formation of the $E_i^\#$ complexes is that the i-face is designed to make contact with an organized interface and therefore also has a tendency to make contact with the head groups and cooperatively bind multiple monodisperse amphiphiles. For example, cooperative binding of monodisperse decylsulfate (A) to PLA2 gives three discrete premicellar $E_i^\#$ ($i = 1$, 2, and 3) complexes with a stoichiometry

* To whom correspondence should be addressed. Telephone: +1-302-831-2968. Fax: +1-302-831-6335. E-mail: mkjain@udel.edu.
‡ University of Delaware.
§ Uppsala University.

[1] Abbreviations: cmc, critical micelle concentration; DC_7PC, 1,2-diheptanoyl-phosphatidylcholine; iso-PLA2, natural variant of PLA2 with T12A, D17H, L20M, and N70E substitutions; HEPES, 4-(2-hydroxyethyl)-1-piperazineethanesulfonic acid; i-face, interface binding surface of an interfacial enzyme; NBS, *N*-bromosuccinimide; PLA2, secreted type IB phospholipase A_2 from pig pancreas; STD, saturation-transfer difference.

10.1021/bi702164n CCC: $40.75
Published on Web 02/08/2008

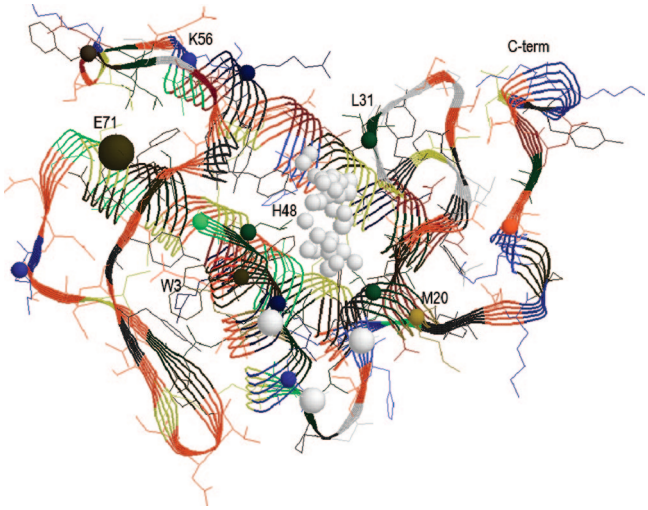

FIGURE 1: Key features of the i-face surrounding the active site slot of PLA2 (*7*). The desolvated center of the i-face makes short-range (<5 Å) contact with the interface by ligand substitution. The charged groups (K53, K56, K63, K120, K121, and E71) are within the Debye length of the electrical double layer on the interface and also 5−8 Å away from the desolvated i-face. The substrate binding slot in the middle of the i-face contains the competitive inhibitor MJ33 (gray balls). Large gray balls are the three phosphates in the anion-assisted dimer structure [Protein Data Bank (PDB) 1FXF] used for this representation of the i-face. Coplanar C_α atoms of some of the residues (shown as the colored balls) are Ala-1 (green), Leu-2 (black), Trp-3 (black), Lys-6 (blue), Lys-10 (blue), Leu-19 (black), and Met-20 (olive).

Scheme 1

$$E \underset{n_1, K_1^{\#}}{\overset{+N_1 A}{\rightleftharpoons}} E_1^{\#} \underset{n_2, K_2^{\#}}{\overset{+N_2 A}{\rightleftharpoons}} E_2^{\#} \underset{n_3, K_3^{\#}}{\overset{+N_3 A}{\rightleftharpoons}} E_3^{\#} \overset{+A^*}{\rightleftharpoons} E^*$$

of N_i amphiphiles per enzyme, Hill numbers n_i, and dissociation constant $K_i^{\#}$ (Scheme 1) (*19, 26–28*).

The micelle-bound (interfacial) E* complex is formed above the critical micelle concentration (cmc) of the amphiphile. Values of $K_i^{\#}$ are higher for the higher complexes, and they will also form in that order. This description works well for the fits because under most conditions the changes in the relative signal intensity (a_i) for the successive complexes are well-separated. Other possibilities can not be ruled out. For example, with well-separated steps, it is not possible to unequivocally distinguish whether the complexes are formed independently of each other or by contiguous clustering of amphiphiles to the previous complex.

Results in this paper show that cooperative amphiphile binding to the i-face of PLA2 does not require calcium or inhibitor binding to the active site. The amphiphile binding is driven by hydrophobic interactions with a modest contribution from the electrostatic compensation of the head group interactions. The saturation-transfer difference (STD) NMR epitope of decylsulfate bound to the higher complexes increasingly resembles that of decylsulfate in the micellar E* complexes. The STD signatures of bound amphiphiles also provide direct evidence for the clustering of decylsulfate on PLA2 as also inferred by independent methods that monitor the changes on PLA2 (*18, 19, 27*). Together, these results show that decylsulfate binding to the i-face of PLA2 is a sequential, cooperative, and contiguous process. We also discuss the possibility that the cooperative amphiphile binding along the i-face to form discrete $E_i^{\#}$ could be related to the allosteric effect of the interface on the active-site events.

EXPERIMENTAL PROCEDURES

Materials, methods, and specific details of established protocols and conditions to characterize kinetic parameters for PLA2 on DMPM vesicles and for the biophysical characterization of the premicellar complexes of PLA2 are published previously (*14, 19, 26–29*). Typically, the kinetic measurements were made at room temperature at 24 °C and pH 8. Conditions for the fluorescence and NMR measurements are described below. The K6M, K10M, and K6M/K10M mutants were expressed and characterized as described previously (*17*). The late Professor Verheij (Utrecht) provided the precharacterized iso-PLA2 and the M8L/M20L mutant (*30*). The cmc of decylsulfate under our measurement conditions is 4.5 mM and changes little in <2 mM calcium.

Decylsulfate Binding Isotherm from the Fluorescence Change. The fluorescence emission measurements were carried out on a SLM-Aminco AB2 instrument set in the ratio mode with 4 nm slit widths and excitation at 280 nm. Emission was at 333 nm for the Trp signal. The noise level in the intensity values was typically <1%, with an integration time of 4 s. Results with the W3F mutant showed that >97% of the fluorescence signal from PLA2 is from Trp-3. Other conditions are given in the figure captions and text.

Experimental protocols, theory, and analysis for the interpretation of the decylsulfate binding model in Scheme 1 are established (*27*). The titration curves were generated by successive addition of 0.5−5 μL solution of decylsulfate to 2 μM PLA2 in 1.6 mL of stirred buffer, with an equilibration time of 3–5 min. The stepwise change in the Trp-3 emission intensity with the formation of $E_i^{\#}$ with the increasing concentration, c_f, of monodisperse decylsulfate is analytically described as (*27*)

$$\delta F = \frac{(c_f/K_1^{\#})^{n_1}\{a_1 + (c_f/K_2^{\#})^{n_2}[a_2 + a_3(c_f/K_3^{\#})^{n_3}]\}}{1 + (c_f/K_1^{\#})^{n_1}\{1 + (c_f/K_2^{\#})^{n_2}[1 + (c_f/K_3^{\#})^{n_3}]\}} \quad (1)$$

Fit parameters for the decylsulfate titration curve were obtained (Origin or MathCad programs) using the normalized intensity change δF ($=F/F_o - 1$), where F_o is the intensity of the enzyme solution and F is the intensity in the presence of decylsulfate. All $K_i^{\#}$ values are given in the millimolar concentration unless mentioned otherwise. The intensity change parameter a_i for the complex $E_i^{\#}$ is relative to the E form. For example, a_2 of +0.5 means that the emission intensity of $E_2^{\#}$ is 50% higher compared to that of E. For adequate fits without significant covariance (<0.90), it is necessary that the successive a_i values differ by more than 0.1. On the basis of the standard deviation under these conditions, uncertainty in the estimated parameters is typically 10%. On the basis of a covariance of >0.9, an uncertainly of 30% is likely, where the signal intensity (a_i) is <0.15. We have not included the parameter estimates where the uncertainty is likely to be >30%. An uncertainty of up to 30% in certain parameters has also been observed in different runs. Possible sources of run-to-run variability include the effect of the order of addition and slow drift in the Trp-3 fluorescence from the higher complexes presumably because of self-aggregation of premicellar complexes

(*19*). Controls showed that more than a 2-fold change in a parameter value is significant.

STD NMR and Proton Nuclear Spin–Lattice Relaxation Rates. All NMR measurements were made at 15 °C in 20 mM 4-(2-hydroxyethyl)-1-piperazineethanesulfonic acid (HEPES) buffer in D_2O (99%) at pH 6.9 with the indicated concentrations of wild-type PLA2 and decylsulfate. The proton nuclear spin–lattice relaxation rates and STD measurements were carried out on a Bruker NMR spectrometer operating at 600.13 MHz and equipped with a triple-resonance CryoProbe. The standard inversion recovery method was used for the T_1 measurement. Conditions for enhanced STD−NMR measurements were selected on the basis of published experimental and theoretical considerations (*31–35*). Typically, the pulse sequence starts with a train of Gaussian-shaped RF saturation pulses (50 ms with an irradiation power of 87 Hz) to saturate nuclear magnetization for the protein resonances. The number of pulses determines the saturation time. The saturation time of 0.5 s was used unless noted otherwise. The RF saturation pulse train was followed by a hard 90° pulse, a $T_{1\rho}$ filter with a strength of 4960 Hz (40 ms) for removing residual protein signals, and a WATERGATE sequence (*36*) for suppressing the solvent signals before data acquisitions. The proton NMR resonance range for PLA2 is from −0.2 to 9.5 ppm and from 0.5 to 4 ppm for decylsufate. The frequency of the Gaussian pulse train was set to the off-resonance frequency at 30 ppm and the on-resonance-frequency at 6.7 ppm unless noted otherwise. The STD−NMR signal results from the difference between the NMR signals with on- and off-resonance irradiation. The subtraction was carried out by a phase-cycling scheme. The STD spectra were co-added and averaged from 256 to 6144 scans depending upon the concentration of decylsulfate, the PLA2 concentration, and the RF irradiation time.

Monitoring the Active-Site Occupancy by the Protection Method. The half-time for alkylation of the active-site residue His-48 by *p*-nitro-phenacylbromide is more than 30-fold longer if calcium alone or together with an inhibitor is bound to the active site of PLA2. The increase in the half-time provides a reliable quantitative measure of calcium bound to the active site with or without an inhibitor (*37, 38*).

RESULTS

Binding of Decylsulfate to the N-Terminus Mutants. PLA2 forms $E_i^{\#}$ complexes (Scheme 1) with monodisperse decylsulfate (cmc = 4.5 mM). Fluorescence titration curves for PLA2 or its natural variant iso-PLA2 (with T12A, D17H, L20M, and N71E substitutions) with decylsulfate in Figure 2 show well-resolved two or three stepwise changes in the Trp-3 emission intensity. As modeled in eq 1, the signal intensity is a quantitative measure of decylsulfate binding to the i-face (*27*). The value of a_i depends upon the change in the local dielectric and quenching environment that can not be assigned to a specific structural feature (*17, 39*). The Hill number n_i is the minimum number of amphiphiles in $E_i^{\#}$. Changes in $K_i^{\#}$ reflect the energetic contributions to the decylsulfate binding. Typically, the a_1 to a_2 difference is significant, but the a_2 and a_3 difference is noticeable, for example, for iso-PLA2 (Figure 2). The changes discussed in this study are for the complexes for which a_i is adequately resolved. Unresolved a_i does not necessarily rule out the formation of other complexes whose Trp-3 signal may not be distinguishable.

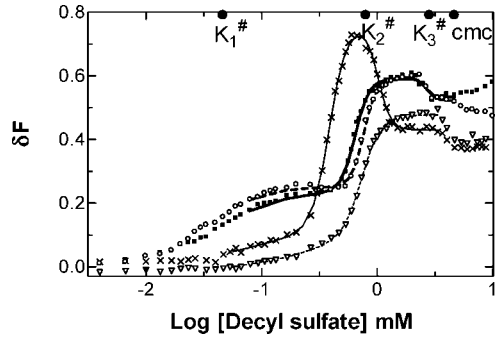

FIGURE 2: Decylsulfate concentration (log scale) dependence of the change in the relative fluorescence intensity (emission at 333 nm and excitation at 280 nm) of 2 μM PLA2 in 1.6 mL of buffer at pH 6.9 containing (○) ethylene glycol bis(2-aminoethyl ether)-*N*,*N*,*N*′,*N*′-tetraacetic acid (EGTA) or (■) 0.5 mM $CaCl_2$. Results for iso-PLA2 are in (▽) EGTA or (×) 0.5 mM $CaCl_2$. The fit (—) parameters $K_i^{\#}$, a_i, and n_i are summarized in Table 1. The cmc and $K_i^{\#}$ for the wild type are marked. Controls with W3F mutant (*17*) showed that tyrosine contributes <3% of the intensity at 333 nm.

Table 1: Decylsulfate Binding Parameters[a] for PLA2 Mutants at pH 6.9 with 0.5 mM Calcium (Ca) or without Calcium (eg)[b]

mutant	+	$K_1^{\#}$ (mM)	$K_2^{\#}$ (mM)	a_1	a_2	n_1	n_2	v_o (s^{-1})
WT	Ca	0.042	0.65	0.24	0.59	1.7	7	270
	eg	0.033	0.79	0.24	0.58	1.7	8	
R6M	Ca	0.02	1.0	0.14	1.0	1.5	7	46
	eg	0.03	1.2	0.15	1.0	1.5	8	
K10M	Ca	0.02	0.86	0.33	0.68	1.4	7	64
	eg	0.03	1.0	0.36	0.59	2	8	
R6M/K10M	Ca	0.2	0.95	−0.06	0.6		4	30
	eg	0.2	1.6	−0.04	0.65		4	
M8L/M20L[c]	Ca		0.64		0.20	2.1	9	185
	eg	0.03	0.80	0.09	0.26	1.3	6	
isoPLA2[c]	Ca	0.2	0.36	0.20	0.77	1	6	65
	eg	0.19	0.72	0.07	0.4	3	5	

[a] Uncertainty is <30%. [b] In 0.48 M NaCl, 10 mM Tris, and 20 mM HEPES at pH 6.9 and 24 °C in the presence of calcium or EGTA. [c] Results from ref *44*.

We characterized the decylsulfate binding to several mutants, in which residues around the anion binding site (*8*) on the i-face (Figure 1) are substituted. As summarized in Table 1, substitution of the cationic residues by methionine on the 1,10 helix (Figure 1) has a modest <5-fold effect on the decylsulfate binding parameters. The effect of R6M and K10M substitution on $K_1^{\#}$ (Table 1) suggests that the stabilizing contribution of cationic R6, K10, or both to the binding of each decylsulfate molecule involved in $E_1^{\#}$ on average is less than 1 kcal/mol. Although energetically weak, other changes associated with such interactions could play a significant role in the allosteric effect of the interface. For example, the 1,10 helix is part of the i-face (*7, 8, 21, 22, 40*), with L2, F5, and L9 on the wall of the active-site slot (*41–43*). Also, in the anion-assisted dimer structure (*8, 44, 45*) R6 (NH2, NH1, and NHϵ), K10 (N_z), L19 (N), and M20 (N) provide ligands for the short-range (<3.5 Å) specific binding of three coplanar sulfate or phosphate anions. Other results (*17, 19, 27*) show that the charge reversal by K53M, K56M, and K120M substitutions also has a modest effect on the decylsulfate binding parameters. In general, these and other substitutions (*15, 17, 46*) on the i-face have a noticeable

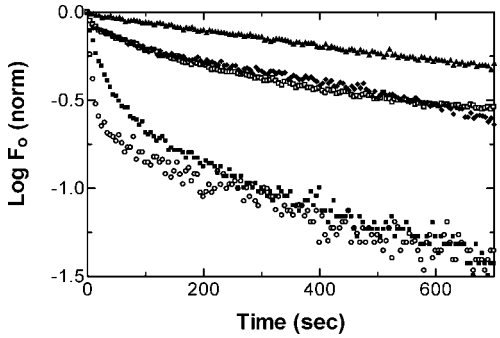

FIGURE 3: Time course of modification (semi-log plot) of Trp-3 of WT PLA2 (2 μM added at $t = 0$) with 0.2 mM NBS at pH 6.9 in 20 mM Tris-HEPES buffer and 24 °C and decylsulfate: 0 mM (E), 0.3 mM ($E_1^\#$), 1.5 mM ($E_2^\#$), 3 mM ($E_3^\#$), and 5 mM (E*).

specific effect on the catalytic parameters, which suggests that the amphiphile binding along the i-face has an allosteric effect on the active-site events. In this paper, we further characterize only the cooperative amphiphile binding along the i-face.

Shielding of Trp-3 from Covalent Modification by N-Bromosuccinimide (NBS). As shown in Figure 3, the time course of the reaction of NBS with free PLA2 is biphasic. The initial rapid quenching is due to the formation of the bromo-tryptophan intermediate. Water accessibility is rate-limiting for the formation of the less fluorescent oxo-tryptophan in the second step (*17*). The half-times for the second step are up to 20-fold longer for the higher complexes in the order $E = E_1^\# < E_2^\# = E_3^\# = E^*$ complexes of PLA2 with decylsulfate. This result is in accordance with the correspondingly decreasing efficiency of the dynamic quenching of Trp-3 with succinimide and also other evidence that shows binding and clustering of decylsulfate on the i-face to shield Trp-3 (*19, 27*). Together, these results show that clustering of decylsulfate on the i-face changes the rate of oxidation of Trp-3 in PLA2 by NBS.

STD NMR Signal from HEPES Buffer. We have used HEPES buffer for the STD NMR investigation. Surprisingly, as shown in spectrum A in Figure 4, the STD signal intensity from 20 mM HEPES buffer alone was significant at saturation times of 0.26−3 s with on-resonance frequencies of 0 or 6.7 ppm. The STD signal from HEPES changes <10% in the presence of PLA2 alone (spectrum B) and <3% in the presence of decylsulfate alone (results not shown). These controls show a small effect of PLA2 or decylsulfate on the STD spectrum of HEPES, as well as the effect of HEPES on the STD signal from decylsulfate or the effect of decylsulfate on HEPES.

Two other control spectra C and D in Figure 4 ruled out an effect of HEPES on the STD signal of decylsulfate from $E_i^\#$. C is the STD spectrum where HEPES spectrum is subtracted. D is the STD spectrum in bicarbonate. These results show a comparable STD signal from decylsulfate in a 15:1 ratio with PLA2 where $E_2^\#$ would predominate. These controls show that the STD behavior of decylsulfate in the $E_2^\#$ complex is not influenced by HEPES buffer. Note that the absolute STD intensities from decylsulfate are somewhat lower in bicarbonate than in HEPES buffer. It is likely to be associated with some step in Scheme 2. It is however inconsistent with the suggestion that sulfonate of HEPES competes out decylsulfate bound to PLA2. Controls with

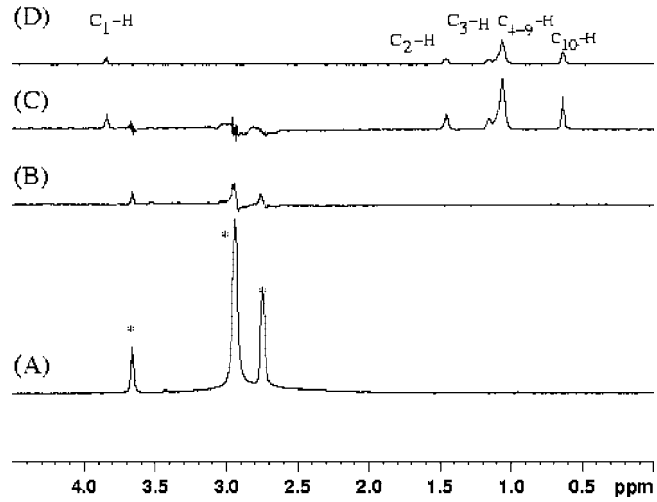

FIGURE 4: (A) STD spectrum of 20 mM HEPES buffer alone. The difference spectrum obtained by subtracting spectrum A from the STD spectrum in 20 mM HEPES buffer of 10 μM PLA2 (B) alone or (C) with 0.75 mM decylsulfate. (D) The STD spectrum of 10 μM PLA2 with 0.75 mM decylsulfate in 20 mM bicarbonate buffer. Spectra were obtained under identical conditions and displayed at the same magnification. Absolute intensity values in C and D are different, however the intensities relative to C_1−H are comparable. Saturation time of 2.1 seconds was used in these measurements for an enhanced STD signals. Asterisks (*) represent the proton resonances of HEPES buffer.

Scheme 2

$$\begin{array}{ccc} E_i^\#(N_i)' & \xrightarrow{k_{-1}} & E_i^\#(N_i-1)' + A' \\ \uparrow \text{RF} & & \downarrow \text{slowest step} \\ E_i^\#(N_i) & \xleftarrow{k_1} & E_i^\#(N_i-1) + A \end{array}$$

other premicellar complexes showed that HEPES does not change the STD signal in any $E_i^\#$ complex.

The STD signal from HEPES buffer has not been reported before, and we do not have an explanation for it. However, with both on and off resonance at 30.0 ppm, HEPES showed only a weak residual signal resulting from the spectral subtraction. Also HEPES dissolved in DMSO did not give any STD signal. However, a significant STD signal was observed with HEPES dissolved in DMSO containing 25 vol % D_2O.

STD NMR of $E_i^\#$ Complexes. STD spectra have been used to map the binding epitope of the ligand in complexes where 1:1 stoichiometry is independently established (*33, 35, 47*). A STD NMR spectrum is a map of the "memory" of the magnetization transferred to the bound ligand in a RF saturated complex of the protein. It provides unequivocal qualitative evidence for the formation of the complex. The STD peak intensities for different proton resonances contain information about the differences in their respective environments in the complex. Such model-dependent interpretations assume that the STD signal has contributions from the steps of the binding equilibrium as well as the internal dynamics of the complex. The assumptions built into Scheme 1 are also necessary to interpret the STD results from the $E_i^\#$ complexes in Scheme 2.

As outlined in Scheme 2, saturation in RF-irradiated protein is rapidly transferred to the whole protein by spin diffusion. In the complex, the magnetization is also transferred by intermolecular dipolar interactions to the bound

amphiphile molecules. Thus, a subpopulation of the two spin states of the protons of both PLA2 and A′ in $E_i^{\#}(N_i)'$ is saturated. On the sub-millisecond time scale, one or more bound amphiphile molecules would likely dissociate from the $E_i^{\#}(N_i)'$ complex with a $K_i^{\#}$ of $10^{-3}-10^{-8}$ M. In Scheme 2, dissociation of only one A′ is assumed for the formation of $E_i^{\#}(N_i)'$. The measurement protocol is such that if two spectra are taken under exactly the same conditions except the saturation frequencies, one at the on resonance of the protein and the other at the off resonance of the protein, the difference in these two spectra, called the STD spectrum, would result from resonances of A′ transferred during the RF saturation of the complex.

After saturation with the RF pulse sequence, the nuclear spin relaxation for a free small molecule, such as dissociated A′ to A, is expected to be slow. The relaxation of the much larger complex $E_i^{\#}(N_i - 1)'$ to $E_i^{\#}(N_i - 1)$ is expected to be much more rapid. Thus, at the end of the RF saturation pulses, a steady-state population of A′ is created. The resonances of A′ that are saturated by a close contact with the protein will not be sampled by a hard (90°) RF pulse of 10 μs duration. On the other hand, the resonances of A′ that are not saturated through the protein–ligand contact will be detected by the hard pulse. Therefore, the spectrum of A′ with on-resonance irradiation is a collection of resonance intensities dependent upon the progressive saturation transfer to the protons from the protein. The STD spectrum of A′ is obtained by subtraction of this spectrum from a reference spectrum with a saturation frequency setting at an off resonance (30 ppm).

During the pulse sequence the $E_i^{\#}$ complexes are unlikely to dissociate completely. According to Schemes 1 and 2, A′ results from the dissociation of one or more weakly bound A′ bound to $E_i^{\#}(N_i)'$ to form $E_i^{\#}(N_i - 1)'$. Thus, the measured STD spectrum of A′ is similar to the proton NMR spectrum, except that it samples the ensemble average of the magnetization transferred to different ^{1}H in free A′; i.e., the relative intensities of the different protons in the STD spectrum give a nonlinear measure of the extent of the transfer and saturation of magnetization to the individual protons. The absolute signal intensity also depends upon the RF saturation time as well as other equilibrium and kinetic processes: the ligand/protein ratio, temperature, and nuclear spin–lattice relaxation time T_1 of the bound ligand (*33, 48*).

As shown in Figure 5, $E_i^{\#}$ and E* complexes of PLA2 exhibit significant differences in normalized relative STD signal intensities of protons at 1, 2, 3, 4−9, and 10 positions of decylsulfate. On the basis of results in Figure 2, under these conditions, $E_1^{\#}$ would predominate at the 1:3 ratio of protein/decylsulfate, and $E_2^{\#}$ would predominate at the 1:15 ratio of protein/decylsulfate, $E_3^{\#}$ would predominate at the 1:44 ratio of protein/decylsulfate, and E* would predominate at the 1:100 ratio of protein/decylsulfate. The STD signal intensities are also consistent with observed $K_i^{\#}$ in the 0.1−5 mM range (Table 1), with the assumption that the binding is diffusion-limited.

The saturation time of 0.5 s used for the results in Figure 5 is about half of the nuclear spin relaxation time T_1 values for the protons in decylsulfate. As summarized in Table 2, T_1 for the monomer decylsulfate are larger than those for the micelle. This is expected if the increased local order in micelles restricts the segmental motion. Two types of motions

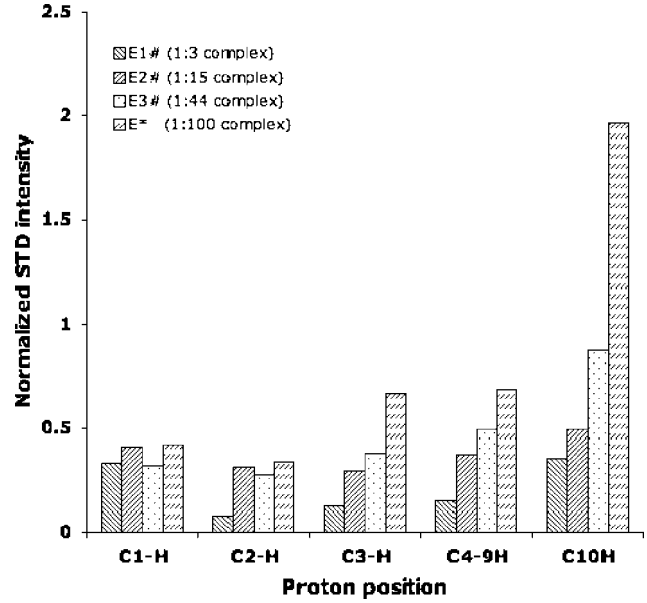

FIGURE 5: STD−NMR signal intensities normalized per proton at 1, 2, 3, 4–9, and 10 positions of decylsulfate. These measurements were carried out with 79 μM wild-type PLA2 and 1:3 ($E_1^{\#}$), 1:15 ($E_2^{\#}$), 1:44 ($E_3^{\#}$), and 1:100 (E*) mole ratio of decylsulfate. The saturation time was 0.51 s. Uncertainty (error bar) in these relative intensity values is <3%. Measured ^{1}H spin–lattice relaxation times (T_1) are given in Table 2.

are often considered (*49–51*). The slow motions with a correlation time of nanoseconds are assigned to the tumbling of aggregates, and the fast motions with correlation times of sub-nanoseconds are assigned to the segmental motions, including bond rotations. In an organized aggregate, the segmental motions are more restricted and play a significant role in the intermolecular dipole–dipole cross-relaxation. Thus, increased efficiency of the intermolecular dipole–dipole interactions in the micelle or complexes would result in lower T_1 values. An increase in T_1 toward the methyl end in E* and $E_2^{\#}$ suggests a less restricted motion presumably because ordering of the alkyl chains in the bound and clustered decylsulfate molecules facilitates transfer of the nuclear magnetization. This conclusion is consistent with the STD results with E* and $E_3^{\#}$, where the methyl end of decysulfate molecules is more disordered.

The difference in the relative signal intensities from C−H in different positions (Figure 5) is also likely to have a contribution from differences in the saturation-transfer efficiencies (*34*). For $E_1^{\#}$, the transfer efficiency is highest for C_1-H and decreases for the protons toward the methyl end. This could be due to a change in the internal dynamics, and also if compared to the rest of the chain, the C_1-H is in better contact with the protein side chains presumably because of the specific interactions of sulfate. This trend is weaker for $E_2^{\#}$, and not apparent in $E_3^{\#}$ and E*, where the relative signal intensity for the C_4-C_9 and C_{10} protons is significantly higher. Such differences suggest that the binding and exchange dynamics of the most weakly bound decylsulfate is different in these complexes. For the higher complexes, E* and $E_2^{\#}$, the relaxation data (Table 2) also support a faster exchange toward the methyl end of the decylsulfate molecules.

Together, these results extend the interpretation of the result from Figure 2 and elsewhere (*19, 27*) to suggest that

Table 2: Proton Spin–Lattice Relaxation Times T_1 (in Seconds) of Decylsulfate

	C_1−H	C_2−H	C_{3-9}−H	C_{10}−H
monomer (3 mM)	1.141 ± 0.002	0.932 ± 0.003	1.071 ± 0.002	2.045 ± 0.002
$E_2^{\#}$ (15:1)	0.97 ± 0.02	1.06 ± 0.02	0.99 ± 0.02	1.22 ± 0.01
E* (100:1)	1.01 ± 0.01	1.04 ± 0.01	1.07 ± 0.02	1.10 ± 0.01
micelle (50 mM)	1.022 ± 0.002	0.808 ± 0.001	0.883 ± 0.002	1.410 ± 0.002
micelle (without O_2)	0.997 ± 0.005	0.808 ± 0.003	0.888 ± 0.002	1.417 ± 0.004

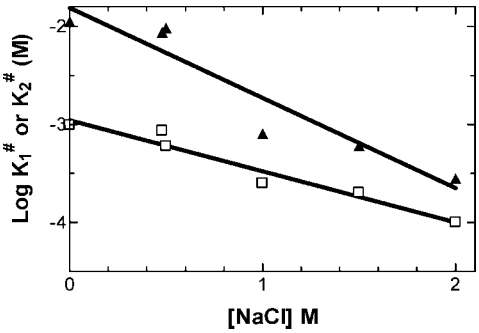

FIGURE 6: NaCl concentration dependence of (□) log $K_1^{\#}$ or (▲) log $K_2^{\#}$ for octylsulfate bound to PLA2 in 1 mM EGTA and 10 mM Tris at pH 8.0. The slope of the linear fit for $K_1^{\#}$ ($r^2 = 0.95$) is –0.52 ± 0.06. For $K_2^{\#}$ ($r^2 = 0.90$), the slope is −0.92 ± 0.15. The effect of calcium on these curves (results not shown) is modest. The $K_i^{\#}$ values were obtained by fluorescence measurements analogous to those shown in Figure 2. Statistical uncertainty in these values is typically 10%, with no noticeable change in the Hill number n.

cooperative binding of decylsulfate in the successive $E_i^{\#}$ complexes (Scheme 1) is contiguous to the ones already bound to the complex. Also, the motional dynamics of the successive complexes increasingly resembles the motional dynamics in micelles. This one-dimensional STD method also has certain advantages over the two-dimensional transferred NOE method (*26*).

Salt Effect on Decylsulfate Binding. Self-aggregation of amphiphiles in the aqueous phase generally increases with the salt concentration (*52, 53*). As shown in Figure 6, a similar effect is observed for the premicellar complexes with PLA2. Two effects are at work here. The hydrophobic effect because of the salting-out of alkyl chains at high salt concentrations increases self-aggregation. Also, the electrostatic shielding and counterion binding increase self-aggregation by reducing the head group repulsion. Both of these effects are apparent in Figure 6, where the affinity of octylsulfate (cmc = 31 mM) for the i-face of PLA2 increases with an increasing NaCl concentration (c_i). The effect of c_i on $K_i^{\#}$ is linearly related as

$$\log K_i^{\#} = -k_s c_i + (\log K_i^{\#})_{c=0}$$

The linear fit for $K_1^{\#}$ gives $k_s = 0.53$, and the linear fit for $K_2^{\#}$ gives $k_s = 0.92$ (M^{-1} with c_i in M). A low slope is expected from the hydrophobic effect alone. The higher slope for $K_2^{\#}$ suggests a contribution from electrostatic screening by the counter-cations to the stability of $E_2^{\#}$ containing many more decylsulfate head groups bound to the i-face of each PLA2 ($n_2 > n_1$). With contiguous clustering of amphiphiles, more like charges are brought together, which will increase the effect of shielding by counter-ions. This interpretation is consistent with the salt effect of $k_s = 0.22$ ($r^2 = 0.91$) on the cmc of zwitterionic diheptanoylphosphatidyl-choline compared to $k_s = 0.83$ ($r^2 = 0.93$) for the cmc of decylsulfate (results 3not shown).

Table 3: Effect of Cations on the Decylsulfate Binding Parameters[a] for PLA2 at pH 6.9

cation	$K_1^{\#}$ (mM)	$K_2^{\#}$ (mM)	a_1	a_2	n_1	n_2
none	0.03	0.79	0.25	0.57	1.7	8.3
0.25 mM Ca	0.03	0.72	0.29	0.61	1.6	10
0.5 mM Ca	0.04	0.65	0.24	0.59	1.5	7
1.0 mM Ca	0.05	0.60	0.29	0.65	1.1	8
2 mM Ca	0.05	0.55	0.27	0.67	1.2	9
3 mM Ca	0.04	0.52	0.26	0.65	1.4	9
10 mM Ca	0.05	0.43	0.24	0.63	1.2	11
0.2 mM Sr^{2+}	0.06	0.9	0.18	0.51	1.6	7
0.2 mM Ba^{2+}	0.05	0.8	0.18	0.49	1.1	8
0.2 mM Cd^{2+}	0.04	0.7	0.20	0.67	1.6	6
0.02 mM Co^{2+}	0.07	1.0	0.20	0.53	2.3	8
0.2 mM Cu^{2+}	0.03	1.5	0.20	0.29	2	10
0.2 mM Zn^{2+}	0.07	0.76	0.23	0.49	2.6	8
0.02 mM Tb^{3+}	0.10	0.6	0.40	0.80	1.2	10
0.02 mM Gd^{3+}	0.04	1.1	0.20	0.50	1.1	6

[a] Uncertainty is <30%.

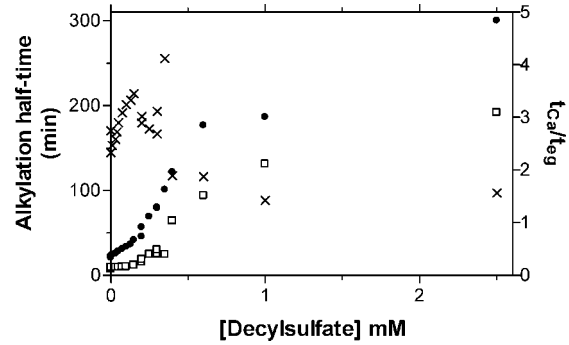

FIGURE 7: Decylsulfate concentration dependence of the alkylation half-time of PLA2 (3 μM) with 2 mM *p*-nitrophenacylbromide (*37*) in (□) cacodylate buffer at pH 6.9 containing 1 mM EDTA (t_{eg}) or (●) 0.5 mM $CaCl_2$ (t_{Ca}). (×) t_{Ca}/t_{eg} ratio (=1 + [Ca]/K_{Ca}).

Calcium Is Not Required for the Decylsulfate Binding to the i-Face. Calcium bound via D49 is obligatorily required for the substrate binding and also for the chemical step (*54, 55*) mediated by the H49−D99 pair (*54, 56*). K_{Ca}^{1} is 0.32 mM for the E form at pH 8 (*37*). As summarized in Table 3, the decylsulfate binding parameters change modestly in the presence of 0.2 mM concentration of certain di- and trivalent cations. The 2.5-fold difference in $K_2^{\#}$ is significant, with the lowest value for Tb^{3+} and the highest for Cu^{2+}. This change could be via the low-affinity cation-binding site (*57*), or the decylsulfate binds to the active site in the presence of certain cations that lower the apparent $K_i^{\#}$ values. However, a negligible effect of most of the cations in Table 3 suggest that decylsulfate binding to the i-face does not require calcium in the active site, which is also consistent with the result that decylsulfate binding does not correlate with the effect of the cation on the active-site events (*55*).

Alkylation Half-Time for H48 of PLA2 in $E_i^{\#}$. As shown in Figure 7, the half-time for inactivation of PLA2 by alkylation of the catalytic residue H48 changes with the decylsulfate concentration in the presence or absence of

calcium. The alkylation time increases <2-fold with the formation of $E_1^\#$ below 0.3 mM decylsulfate. The half-time changes sharply with the formation of $E_2^\#$ between 0.4 and 1 mM decylsulfate. Such a change associated with the formation of $E_2^\#$ is related to a change in the reactivity or reagent accessibility of H48. The effect of calcium on the relative alkylation time is not due to the calcium-dependent binding of decylsulfate to the active site. However, as shown in Figure 7, the t_{Ca}/t_{eg} ratio ($=1 + [Ca]/K_{Ca}$) changes systematically but modestly with the decylsulfate concentration. Throughout the range, the apparent K_{Ca} remains in the 0.25−0.4 mM range, showing that there is little cross-talk between calcium in the active site and decylsulfate on the i-face. Because of longer alkylation times, there is greater uncertainty in the t_{Ca}/t_{eg} ratio at the higher decylsulfate concentrations. The interpretation of the low affinity of decylsulfate for the active site is also consistent with the estimated dissociation constant of >0.5 mol fraction for decylsulfate bound to the active site of E* on micelles of a zwitterionic neutral diluent (*37, 55*).

DISCUSSION

Accumulated evidence shows that the $E_i^\#$ complexes of interfacial enzymes are surrogates for some of the structural and functional states formed during the E to E* change or for the states that may coexist in equilibrium with E* at the interface (*15, 19, 26*−*29*). This is consistent with the interfacial kinetic paradigm that the i-face and the active-site events are separate but allosterically coupled (*5, 6, 54*). Results in this paper show that the formation of E* or $E_i^\#$ complexes of PLA2 does not require the occupancy of the active site or the binding of the catalytic calcium. In these complexes, amphiphiles presumably bind along the i-face, and each of the $E_i^\#$ states is different from each other or E* at least in some identifiable way, including a difference in the STD signatures of bound decylsulfate (Figure 5). The significance of these results is developed below to elaborate a better understanding of the premicellar complexes.

Dynamics of Decylsulfate Binding to PLA2. The STD signatures of decylsulfate from $E_i^\#$ complexes are in qualitative accordance with Scheme 1 and the results obtained by monitoring the protein or probe signals. Results in Figures 4 and 5 provide reliable probe-free qualitative information about bound amphiphile. The relative signal intensities also provide the epitope information of the bound amphiphiles. However, absolute intensities can not be interpreted to obtain quantitative information about the stoichiometry or stability of the complexes. The simplest model that emerges is that in analogy with the micellization behavior. The cooperativity of $E_i^\#$ formation is primarily due to contiguous amphiphile−amphiphile interactions, presumably along the i-face of PLA2. Whether or not a change in the protein conformation also occurs does not change the conclusion.

Results in Figure 5 show that the STD environment of the most weakly bound decylsulfate molecules in the $E_i^\#$ and E* complexes is noticeably different. It is because according to Schemes 1 and 2 the steady-state population of A′ is likely to be representative of the amphiphiles that are most weakly bound in the $E_i^\#(N_i)A'$ complex. The nuclear spin saturation transfers to A′ occur while it is in contact with the protein. When the irradiation time is kept less than T_1, different amphiphile protons are magnetized to different extents. Use of a saturation time of 0.5 s that is less than half of T_1 (Table 2) is an adequate compromise (*34*). It is because the nuclear spin relaxation rate of A′ to A starts to have a significant effect on the STD signal intensity if the saturation time is long compared to T_1. The signal would be weak if the saturation time is too short such that the saturation transfer is incomplete.

The plot of the integral of STD peaks normalized to per proton shows that the signal intensities for the protons toward the methyl end of the decyl chain increase for the higher complexes as also shown by the spin–lattice relaxation rates in Table 2. Greater flexibility toward the methyl end of the chain may lead to greater disorder and longer relaxation time T_1. Also, the methyl group with three attached protons is likely to give a stronger STD−NMR signal. Considering all such factors, our interpretation is that the environment of the methyl end of decylsulfate in $E_1^\#$ and $E_2^\#$ is noticeably different than in the higher complexes and possibly in the micelles without protein. In the STD spectrum of the $E_1^\#$ (at 1:3 protein/amphiphile) complex, the relative intensity of C_1−H is noticeably greater than that of the other protons. This would be expected if decylsulfate is bound through sulfate. This trend is weaker for $E_2^\#$ (1:15) if additional decylsulfate molecules are not as tightly bound through sulfate but are clustered in the same way. In the higher complexes, additional amphiphiles will even more weakly bind to the same cluster, presumably because their head-group repulsion is not adequately compensated by the protein (Figure 6). In short, STD results show that the formation of the higher complexes occurs by decylsulfate binding contiguously to the clustered amphiphiles.

Short-Range Interactions along the i-Face. The Hill cooperativity of the amphiphile binding monitored as the changes in Trp-3 emission and also the STD−NMR signatures suggest that the underlying structural changes occur in discrete steps. We have suggested that in E* the contact region along the i-face is desolvated by the short-range specific ligand substitution reactions (*27*) and that such interactions may not necessarily be identical in E* and $E_i^\#$ complexes (*7, 17, 22*). In these ligand substitution reactions, water of solvation is replaced with the polarizable ligands on the i-face of E and on the amphiphile head groups. Besides such enthalpic contributions, the entropic hydrophobic effect from the cooperative clustering of the alkyl chains may also compensate for modest head-group repulsion. All together, multiple short-range ligand substitution reactions over a large area of the i-face (Figure 1) could account for the interaction energy of well over 20 kcal/mol for the stability of E* of PLA2 (*7*).

$E_i^\#$ Formation versus Micellar Aggregation. The equilibrium underlying the formation of the premicellar complexes (eq 1) differs from the monomer−micelle equilibrium (*6*). While micelle concentration is constrained only by the total amount of amphiphile, the premicellar complexes are constrained also by the total concentration of enzyme. Thus, if the amphiphile binding is tight, the amphiphile depletion would influence the shape of the titration curve. It is taken into account for the STD results.

For micelles (with $X = 1$), cmc is determined by the monomer concentration C_{mono}. If we describe the micellization as $n \times A \rightarrow M$ as the simultaneous joining of n

monomers, we get the equilibrium relationship [M] = $(C_{mono}/K')^n$. In the limit of large n and $C_{total} > K'$, this has the solution $C_{mono} \approx K'$ (approximately but very nearly). If the results were exact, it would give the micelle concentration [M] = 1 always, which of course is not the case. Therefore, for a large aggregation number n for micelles, cmc = K' holds. The main point is that $K_i^\#$ and cmc therefore are constants on exactly the same footing. In the case where enzyme is in excess, premicellar complexes with large n will behave similarly with $C_{mono} \approx K_i^\#$. When premicellar complexes are large enough, they will automatically be described in the same way as micelles. We have not considered possible contributions of the self-aggregation of the $E_i^\#$ complexes (*27*).

Hill Cooperativity for the Binding of Decylsulfate to PLA2. Sequential formation of discrete $E_i^\#$ complexes implies that decylsulfate molecules cooperatively bind to distinct structural regions. Hill cooperativity of $n_1 = 1.7$, $n_2 = 6-8$, and $n_3 = 5-10$ suggest that at least 2–3, 8–10, and 20 decylsulfate molecules are bound per PLA2 in these complexes. STD results show that these regions are contiguous on the i-face (Figure 1). The protection results as well as the spectroscopic differences between the complexes of the mutants show a change in the protein. It suggests an allosteric effect of the cooperative amphiphile binding to the i-face on the active site that remains to be characterized. Likely scenarios are considered below.

In $E_1^\#$, the dissociation constant of decylsulfate in the absence of calcium is $K_1^\# = 40$ μM with the Hill number $n_1 = 1.7$. More than one decylsulfate would be bound but none to the active site. A possible basis for the fractional Hill cooperativity n_1 is that two molecules of decylsulfate are bound in $E_1^\#$, but both singly bound substates contribute to the Trp-3 signal. Also, cooperativity is not complete if the dissociation constant for a single decylsulfate is not large enough. On the basis of these observations, we suggest that the initial binding of 1−3 amphiphiles allosterically controls the i-face and the catalytic site interaction and that its functional consequences depend upon the structure of the amphiphile possibly via the 57–72 loop (*18*).

Cooperative amphiphile binding in $E_2^\#$ could take place in a number of ways. The simplest scenario is that the amphiphiles in the $E_1^\#$ simply form a core or nucleus around which $E_2^\#$ can form. In this model, for the i-face cooperativity and its allosteric effect on the active site, the individual amphiphiles stabilize binding of more just through neighbor interactions. There could be some allosteric change in the enzyme that promotes binding to the i-face as well as the active site. In analogy with the hemoglobin model, another possibility is that in the $E_1^\#$ to $E_2^\#$ step binding of the first few (n_1) amphiphiles might trigger a conformational change that opens up a whole binding region for the remaining 6–10 amphiphiles. The 62–66 loop is a likely candidate for such a change. If there are such allosteric effects, they come into play between the successive $E_i^\#$ states, so that $E_1^\#$ formation could allosterically trigger $E_2^\#$ formation. It is possible that the additional changes related to the loop also occur during the formation of $E_3^\#$ and E* on micelles. It should be possible to characterize such atomic level changes by NMR methods.

ACKNOWLEDGMENT

We thank Professor Tatyana Polenova and Cecil Dyboski for numerous discussions during the progress of the NMR studies and comments on the manuscript.

REFERENCES

1. Yu, B. Z., Berg, O. G., and Jain, M. K. (1999) Hydrolysis of monodisperse phosphatidylcholines by phospholipase A_2 occurs on vessel walls and air bubbles. *Biochemistry 38*, 10449–10456.
2. Homan, R., and Jain, M. K. (2000) In *Intestinal Lipid Metabolism* (Mansbach, C. M., Tso, P., and Kuksis, A. E., Eds.) pp 81–104, Plenum Publishing, New York.
3. Upreti, G. C., and Jain, M. K. (1980) Action of phospholipase A_2 on unmodified phosphatidylcholine bilayers: Organizational defects are preferred sites of action. *J. Membr. Biol. 55*, 113–121.
4. Apitz-Castro, R., Jain, M. K., and De Haas, G. H. (1982) Origin of the latency phase during the action of phospholipase A_2 on unmodified phosphatidylcholine vesicles. *Biochim. Biophys. Acta 688*, 349–356.
5. Berg, O. G., Gelb, M. H., Tsai, M. D., and Jain, M. K. (2001) Interfacial enzymology: The secreted phospholipase A_2-paradigm. *Chem. Rev. 101*, 2613–2654.
6. Berg, O. G., and Jain, M. K. (2002) *Interfacial Enzyme Kinetics*, Wiley, London, U.K.
7. Ramirez, F., and Jain, M. K. (1991) Phospholipase A_2 at the bilayer interface. *Proteins: Struct., Funct., Genet. 9*, 229–239.
8. Pan, Y. H., Epstein, T. M., Jain, M. K., and Bahnson, B. J. (2001) Five coplanar anion binding sites on one face of phospholipase A_2: Relationship to interface binding. *Biochemistry 40*, 609–617.
9. Yu, B. Z., Pan, Y. H., Janssen, M. J., Bahnson, B. J., and Jain, M. K. (2005) Kinetic and structural properties of disulfide engineered phospholipase A_2: Insight into the role of disulfide bonding patterns. *Biochemistry 44*, 3369–3379.
10. Jain, M. K., Egmond, M. R., Verheij, H. M., Apitz-Castro, R., Dijkman, R., and De Haas, G. H. (1982) Interaction of phospholipase A_2 and phospholipid bilayers. *Biochim. Biophys. Acta 688*, 341–348.
11. Jain, M. K., Rogers, J., Jahagirdar, D. V., Marecek, J. F., and Ramirez, F. (1986) Kinetics of interfacial catalysis by phospholipase A_2 in intravesicle scooting mode, and heterofusion of anionic and zwitterionic vesicles. *Biochim. Biophys. Acta 860*, 435–447.
12. Berg, O. G., Yu, B. Z., Rogers, J., and Jain, M. K. (1991) Interfacial catalysis by phospholipase A_2: Determination of the interfacial kinetic rate constants. *Biochemistry 30*, 7283–7297.
13. Jain, M. K., Yu, B. Z., and Berg, O. G. (1993) Relationship of interfacial equilibria to interfacial activation of phospholipase A_2. *Biochemistry 32*, 11319–11329 [published erratum appears in (1994) *Biochemistry 33*, 8618].
14. Berg, O. G., Rogers, J., Yu, B. Z., Yao, J., Romsted, L. S., and Jain, M. K. (1997) Thermodynamic and kinetic basis of interfacial activation: Resolution of binding and allosteric effects on pancreatic phospholipase A_2 at zwitterionic interfaces. *Biochemistry 36*, 14512–14530.
15. Yu, B. Z., Poi, M. J., Ramagopal, U. A., Jain, R., Ramakumar, S., Berg, O. G., Tsai, M. D., Sekar, K., and Jain, M. K. (2000) Structural basis of the anionic interface preference and k_{cat}^* activation of pancreatic phospholipase A_2. *Biochemistry 39*, 12312–12323.
16. Rogers, J., Yu, B. Z., Tsai, M. D., Berg, O. G., and Jain, M. K. (1998) Cationic residues 53 and 56 control the anion-induced interfacial k_{cat}^* activation of pancreatic phospholipase A_2. *Biochemistry 37*, 9549–9556.
17. Tsai, Y., Yu, B.-Z., Wang, Y., Chen, J. W., and Jain, M. K. (2006) Desolvation map of the i-face of phospholipase A_2. *Biochim. Biophys. Acta 1758*, 653–665.
18. Yu, B. Z., Apitz-Castro, R., Jain, M. K., and Berg, O. G. (2007) Role of the 57–72 loop in specific interaction of bile salts with pancreatic IB phospholipase A_2: Regulation of fat and cholesterol homeostasis. *Biochim. Biophys. Acta 1768*, 2478–2490.
19. Yu, B. Z., Apitz-Castro, R., Tsai, M. D., and Jain, M. K. (2003) Interaction of monodisperse anionic amphiphiles with the i-face of secreted phospholipase A_2. *Biochemistry 42*, 6293–6301.
20. Jain, M. K., DeHaas, G. H., Marecek, J. F., and Ramirez, F. (1986) The affinity of phospholipase A_2 for the interface of the substrate and analogs. *Biochim. Biophys. Acta 860*, 475–483.
21. Pan, Y. H., Yu, B. Z., Berg, O. G., Jain, M. K., and Bahnson, B. J. (2002) Crystal structure of phospholipase A_2 complex with

the hydrolysis products of platelet activating factor: Equilibrium binding of fatty acid and lysophospholipid-ether at the active site may be mutually exclusive. *Biochemistry 41*, 14790–14800.
22. Bahnson, B. J. (2005) Structure, function and interfacial allosterism in phospholipase A_2: Insight from the anion-assisted dimer. *Arch. Biochem. Biophys. 43*, 96–106.
23. Jain, M. K., and Vaz, W. L. (1987) Dehydration of the lipid−protein microinterface on binding of phospholipase A_2 to lipid bilayers. *Biochim. Biophys. Acta 905*, 1–8.
24. Jain, M. K., Rogers, J., Marecek, J. F., Ramirez, F., and Eibl, H. (1986) Effect of the structure of phospholipid on the kinetics of intravesicle scooting of phospholipase A_2. *Biochim. Biophys. Acta 860*, 462–474.
25. Rogers, J., Yu, B. Z., and Jain, M. K. (1992) Basis for the anomalous effect of competitive inhibitors on the kinetics of hydrolysis of short-chain phosphatidylcholines by phospholipase A_2. *Biochemistry 31*, 6056–6062.
26. Yu, B. Z., Polenova, T. E., Jain, M. K., and Berg, O. G. (2005) Premicellar complexes of sphingomyelinase mediate enzyme exchange for the stationary phase turnover. *Biochim. Biophys. Acta 1712*, 137–151.
27. Berg, O. G., Yu, B. Z., Chang, C., Koehler, K. A., and Jain, M. K. (2004) Cooperative binding of monodisperse anionic amphiphiles to the i-face: Phospholipase A_2-paradigm for interfacial binding. *Biochemistry 43*, 7999–8013.
28. Berg, O. G., Yu, B. Z., Apitz-Castro, R. J., and Jain, M. K. (2004) Phosphatidylinositol-specific phospholipase C forms different complexes with monodisperse and micellar phosphatidylcholine. *Biochemistry 43*, 2080–2090.
29. Jain, M. K., and Berg, O. G. (2006) Coupling of the i-face and the active site of phospholipase A_2 for interfacial activation. *Curr. Opin. Chem. Biol. 10*, 473–479.
30. Janssen, M. J., Verheij, H. M., Slotboom, A. J., and Egmond, M. R. (1999) Engineering the disulphide bond patterns of secretory phospholipases A_2 into porcine pancreatic isozyme. The effects on folding, stability and enzymatic properties. *Eur. J. Biochem. 261*, 197–207.
31. Angulo, J., Rademacher, C., Biet, T., Benie, A. J., Blume, A., Peters, H., Palcic, M., Parra, F., and Peters, T. (2006) NMR analysis of carbohydrate−protein interactions. *Methods Enzymol. 416*, 12–30.
32. Mayer, M., and Meyer, B. (2001) Group epitope mapping by saturation transfer difference NMR to identify segments of a ligand in direct contact with a protein receptor. *J. Am. Chem. Soc. 123*, 6108–6117.
33. Jayalakshmi, V., and Rama Krishna, N. (2004) CORCEMA refinement of the bound ligand conformation within the protein binding pocket in reversibly forming weak complexes using STD−NMR intensities. *J. Magn. Reson. 168*, 36–45.
34. Yan, J., Kline, A. D., Mo, H., Shapiro, M. J., and Zartler, E. R. (2003) The effect of relaxation on the epitope mapping by saturation transfer difference NMR. *J. Magn. Reson. 163*, 270–276.
35. Meyer, M., and Meyer, B. (1999) Characterization of ligand binding by saturation transfer difference NMR spectroscopy. *Angew. Chem., Int. Ed. 38*, 1784–1788.
36. Piotto, M., Sanudek, V., and Sklenar, V. (1992) *J. Biomol. NMR 2*, 661–664.
37. Yu, B. Z., Berg, O. G., and Jain, M. K. (1993) The divalent cation is obligatory for the binding of ligands to the catalytic site of secreted phospholipase A_2. *Biochemistry 32*, 6485–6492.
38. Jain, M. K., Tao, W. J., Rogers, J., Arenson, C., Eibl, H., and Yu, B. Z. (1991) Active-site-directed specific competitive inhibitors of phospholipase A_2: Novel transition-state analogues. *Biochemistry 30*, 10256–10268.
39. Adams, P. D., Chen, Y., Ma, K., Zagorski, M. G., Sonnichsen, F. D., McLaughlin, M. L., and Barkley, M. D. (2002) Intramolecular quenching of tryptophan fluorescence by the peptide bond in cyclic hexapeptides. *J. Am. Chem. Soc. 124*, 9278–9286.
40. Pan, Y. H., Yu, B. Z., Singer, A. G., Ghomashchi, F., Lambeau, G., Gelb, M. H., Jain, M. K., and Bahnson, B. J. (2002) Crystal structure of human group X secreted phospholipase A_2. Electrostatically neutral interfacial surface targets zwitterionic membranes. *J. Biol. Chem. 277*, 29086–29093.
41. Scott, D. L., Otwinowski, Z., Gelb, M. H., and Sigler, P. B. (1990) Crystal structure of bee-venom phospholipase A_2 in a complex with a transition-state analogue. *Science 250*, 1563–1566 [published erratum appears in (1991) *Science 252*, 764].
42. Thunnissen, M. M., Ab, E., Kalk, K. H., Drenth, J., Dijkstra, B. W., Kuipers, O. P., Dijkman, R., de Haas, G. H., and Verheij, H. M. (1990) X-ray structure of phospholipase A_2 complexed with a substrate-derived inhibitor. *Nature 347*, 689–691.
43. van den Berg, B., Tessari, M., Boelens, R., Dijkman, R., Kaptein, R., de Haas, G. H., and Verheij, H. M. (1995) Solution structure of porcine pancreatic phospholipase A_2 complexed with micelles and a competitive inhibitor. *J. Biomol. NMR 5*, 110–121.
44. Yu, B. Z., Pan, Y. H., Janssen, M. J., Bahnson, B. J., and Jain, M. K. (2005) Kinetic and structural properties of disulfide engineered phospholipase A_2: Insight into the role of disulfide bonding patterns. *Biochemistry 44*, 3369–3379.
45. Epstein, T. M., Yu, B. Z., Pan, Y. H., Tutton, S. P., Maliwal, B. P., Jain, M. K., and Bahnson, B. J. (2001) The basis for k_{cat} impairment in prophospholipase A_2 from the anion-assisted dimer structure. *Biochemistry 40*, 11411–11422.
46. Yu, B. Z., Rogers, J., Tsai, M. D., Pidgeon, C., and Jain, M. K. (1999) Contributions of residues of pancreatic phospholipase A_2 to interfacial binding, catalysis, and activation. *Biochemistry 38*, 4875–4884.
47. Sandstrom, C., Bertean, O., Gemrna, E., Oscarson, S., Kennc, L., and Gronenborn, A. M. (2004) Atomic mapping of the interactions between the antiviral agent cyanovirin-N and oligomannosides by saturation-transfer difference NMR. *Biochemistry 43*, 13926–13931.
48. Jayalakshmi, V., and Krishna, N. R. (2002) Complete relaxation and conformational exchange matrix (CORCEMA) analysis of intermolecular saturation transfer effects in reversibly forming ligand−receptor complexes. *J. Magn. Reson. 155*, 106–118.
49. Wennerstrom, H., Lindman, B., Soderman, O., Drakenberg, T., and Rosenholm, J. B. (1979) ^{13}C magnetic relaxation in micellar solutions. Influence of aggregate motion on T1. *J. Am. Chem. Soc. 101*, 6860–6864.
50. Villeneuve, M., Ootsu, R., Ishiwata, M., and Nakahara, H. (2006) Research on the vesicle−micelle transition by ^1H NMR relaxation measurement. *J. Phys. Chem. B 111*, 17830–17839.
51. Nery, H., Soderman, O., Canet, D., Walderhaug, H., and Lindman, B. (1986) Surfactant dynamics in spherical and nonspherical micelles. A nucelar magntic resonance study. *J. Phys. Chem. 90*, 5802–5808.
52. Cevc, G., and Marsh, D. (1987) *Phospholipid Bilayers: Physical Principles and Models*, John Wiley, New York.
53. Mukherjee, P. P. (1967) The nature of the asociation equilibria and hydrophobic bonding in aqueous solutions of asociation colloids. *Adv. Colloid Interface Sci. 1*, 242–275.
54. Verheij, H. M., Slotboom, A. J., and de Haas, G. H. (1981) Structure and function of phospholipase A_2. *Rev. Physiol. Biochem. Pharmacol. 91*, 91–203.
55. Yu, B. Z., Rogers, J., Nicol, G. R., Theopold, K. H., Seshadri, K., Vishweshwara, S., and Jain, M. K. (1998) Catalytic significance of the specificity of divalent cations as K_S^* and k_{cat}^* cofactors for secreted phospholipase A_2. *Biochemistry 37*, 12576–12587.
56. Verheij, H. M., Volwerk, J. J., Jansen, E. H., Puyk, W. C., Dijkstra, B. W., Drenth, J., and de Haas, G. H. (1980) Methylation of histidine-48 in pancreatic phospholipase A_2. Role of histidine and calcium ion in the catalytic mechanism. *Biochemistry 19*, 743–750.
57. van den Bergh, C. J., Bekkers, A. C., Verheij, H. M., and de Haas, G. H. (1989) Glutamic acid 71 and aspartic acid 66 control the binding of the second calcium ion in porcine pancreatic phospholipase A_2. *Eur. J. Biochem. 182*, 307–313.

BI702164N